ELSEVIER

#### Contents lists available at ScienceDirect

## Colloids and Surfaces A

journal homepage: www.elsevier.com/locate/colsurfa

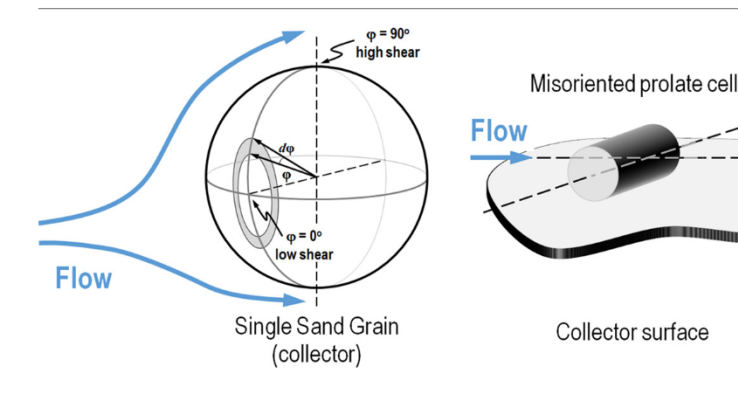


# The mechanistic aspects of microbial transport in porous media

Jianfeng Sun<sup>a</sup>, Ran Ran<sup>a</sup>, Sinan Muftu<sup>a</sup>, April Z. Gu<sup>b</sup>, Kai-Tak Wan<sup>a,\*</sup>

- <sup>a</sup> Department of Mechanical & Industry Engineering, Northeastern University, Boston, MA, USA
- <sup>b</sup> School of Civil and Environmental Engineering, Cornell University, Ithaca, NY, USA





## ARTICLE INFO

Keywords: Bacteria Filtration efficiency Porous medium Ionic concentration DLVO Hydrodynamic shear

## ABSTRACT

A mechanistic model is constructed to account for colloidal filtration by incorporating fundamental intersurface forces between individual particle and collector, geometry and elastic properties of bacteria / particles, and flowrate of the electrolytic medium. Particle adhesion on the collector surface is derived from the DLVO theory based on electrostatic double layers and van der Waals attraction, while particle detachment depends on the hydrodynamic shear. Filtration efficiency,  $\alpha$ , of a conventional packed column is estimated by numerically solving the governing convection-diffusion equation, and is shown experimentally dependent on both ionic concentration and flowrate of the electrolyte contrasting the classical colloid filtration theory. Model bacterial strains of *Aeromonas punctata* and *Raoultella ornithinolytica* were investigated using a conventional packed column test and a homemade microfluidic device. Their behavior were shown to be consistent with the model.

## 1. Introduction

Microbial transport through porous media in subsurface environment is relevant to many aspects of environmental engineering, such as in-situ or enhanced subsurface bioremediation [1], drinking water supplies [2], and filtration process for water and wastewater treatments [3,4]. Flow of particles in a porous medium presents a mathematically involved problem due to the random packing of collectors (e.g. sand grain) and the dendritic percolated channels. Recent computational

studies in 2-dimensional flow through regular an array of cylindrical pillars in the absence of intersurface forces show the necessity of numerical approach and the complications involved [2]. Traditionally, bacterial transportation is modeled by the colloid filtration theory (CFT), in which removal of microbes from a single collector is modeled to be governed by either equilibrium adsorption or the kinetic rate-controlled bacteria attachment to and detachment from the substrate surface [3,4]. CFT addresses three dominant transport mechanisms, namely, diffusion, interception, and sedimentation. When a solution

E-mail address: ktwan@coe.neu.edu (K.-T. Wan).

<sup>\*</sup> Corresponding author.

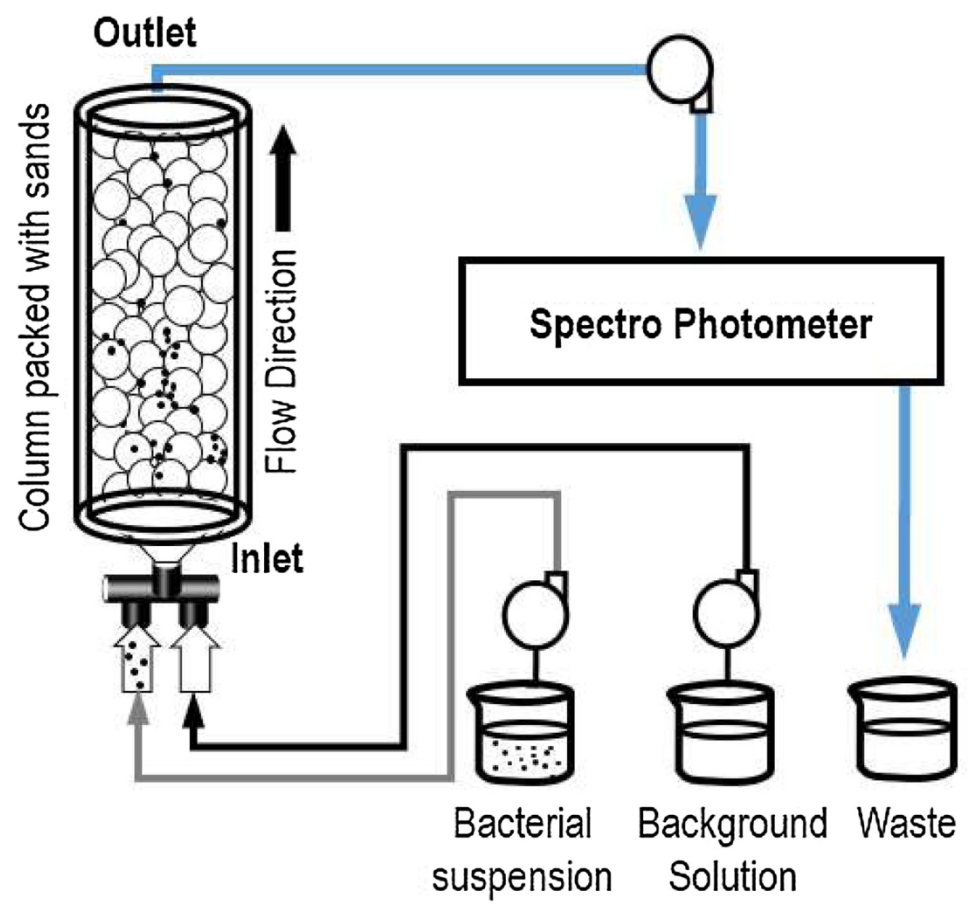


Fig. 1. Schematic of column test. The vertical column is packed with sand grains. Bacterial suspension is pumped through the column from below, while the concentration at the outlet is monitored by spectrophotometer.

with particle concentration,  $C_0$ , passes through a porous bed with length,  $\ell$ , and porosity  $\varepsilon$ , average collector diameter, d, the resulting particle concentration at the efflux, C, is given by

$$\ln \frac{C}{C_0} = -\frac{3}{2}(1-\varepsilon)\alpha\eta \frac{\ell}{d} \tag{1}$$

where  $\eta$  is the single collector collision efficiency typically determined by statistical means [4] or by particle trajectory around the collector surface [5]. Tufenkji [6] incorporated intersurface forces such as van der Waals attraction into  $\eta$ . The attachment efficiency,  $\alpha$ , is the key parameter defined as the ratio of experimental single-collector removal efficiency to the theoretical single-collector contact efficiency. Its value is often determined experimentally using a sand packed column test [3,6–8], and is taken to be the number ratio of particles trapped by the collector to those passing freeing down the column. As the particles enter the column and collide with the collector, some scatter upon impact while others are trapped on the surface. To circumvent sophisticated statistical mechanics that deals with ensembles of sand grains in random stacking configurations and myriad of particles in the flow, collision with a single spherical collector is here taken as the first approximation. The temporo-spatial particle distribution in a filtration column is derived from mass balance of particles with the geometrical constraints of the collector. Once C,  $C_0$ ,  $\ell$ , d and  $\epsilon$  are measured,  $\alpha$  is determined. It is remarkable to note that Eq. (1) relates the macroscopic filtration efficiency to microscopic single collector. The current CFT has been successfully applied to colloidal transportation in porous medium, however, it does not account for a number of relevant quantities: stiffness and geometry of particles, nature of substrate surface [9], and numerous biological factors related to microbial mobility and cell surface characteristics [10-12]. In addition, the often used column test does not account for varying flow rate and the subsequent hydrodynamic shear on the particles adhered to the collector surface, which plays the dominant role of particle detachment that ultimately determines the efficiency of a filtration column and the value of  $\alpha$  [13–15].

In this paper, we propose a fluid mechanics-based model that incorporates intrinsic intersurface forces between particles and collector in the presence of an electrolyte to estimate  $\alpha$ . The particles are taken as cylindrical rods [16] with a surface electrostatic double layer, and their interaction with the collector surface is governed by the classical Derjaguin-Landau-Verwey-Overbeek (DLVO) theory [17]. The velocity field around the adhered particles and the subsequent hydrodynamic shear at specific location on the collector is determined by the multiphysics software COMSOL. The influence of size, geometry, and elastic properties of the particles, as well as their meridional and azimuthal location on the collector surface and orientation to the fluid flow, are also considered. Whether a particle is detached from the substrate therefore depends on the competition between adhesion and shear. The dependence of  $\alpha$  on flow rate and ionic concentration of the liquid medium are then determined. Two specific bacterial strains will be investigated using column test and a homemade microfluidic device, and the measurement will be compared with the prediction. The ranges of flow rate and ionic concentration are matched to typical underground flows.

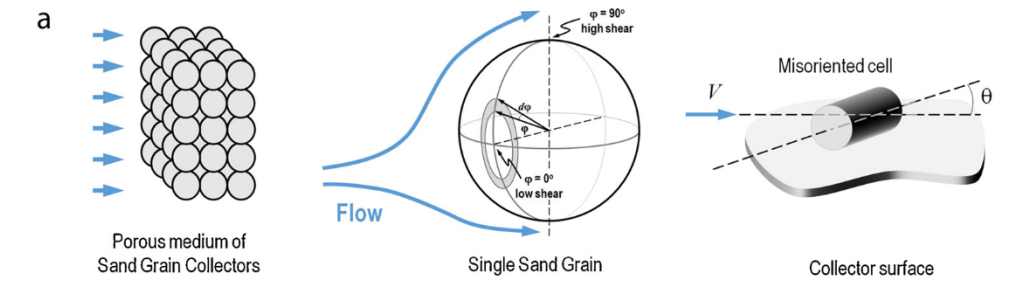
The present model introduces a few new elements to the existing model of colloidal filtration. Firstly, the conventional qualitative description of the intersurface interactions at the cells and collector surface based on DLVO is here *quantified* using a rigorous solid mechanics model. Two additional variables are considered here, namely, ionic concentration of the electrolyte affecting the intersurface interactions,

and geometrical orientation of prolate particles against the flow. The net adhesion force on the substrate is here determined by integrating over the entire cohesive zone at the contact edge using a Green's function approach rather than assuming the particle falling into either the primary or secondary zone [15]. Secondly, a simple criterion is constructed to account for particle detachment due to hydrodynamic shear and the associated torque, contrasting CFT where  $\alpha$  is independent of flowrate. The net torque on a misoriented prolate particle at any point on the spherical collector surface is computed. The present work does not intend to solve entirely colloidal filtration, but to demonstrate that the rigorous solid mechanics and solid-fluid interaction model is consistent with the experiments with two bacterial strains related to human diseases and environmental protection. Limitations and shortcomings of the present model will be discussed in Section 4.

#### 2. Material and methods

#### 2.1. Mechanistic concept and theory

The intersurface interaction will first be derived from DLVO theory, followed by the velocity field and hydrodynamic drag, leading to the filtration efficiency. Fig. 2a shows electrolyte flowing through the porous medium of spherical grain in the packed column, streamline of a steady flow over a single collector sand grain, and microscopic hydrodynamic shear on a single particle adhered onto collector surface. Fig. 2b shows an isolated and stationary cylindrical particle subject to all relevant forces. Particles collide with the collector at a frequency depending on the meridional angle,  $\phi$ , from the polar axis. Hit rate is expected to reach a maximum at the frontal stagnation point at  $\phi=0^\circ$ , and a minimum at the shadowed rear stagnation point at  $\phi=180^\circ$ . The local particle concentration,  $C(\phi,H)$ , at a distance,  $H\,(\,\geq\,R)$ , between the particle and the collector surface, is governed by the classical convection-diffusion equation in spherical coordinates [18],



$$\nabla \cdot (\boldsymbol{u}C) = \nabla \cdot (\boldsymbol{D} \cdot \nabla C) - \nabla \cdot \left( \frac{\boldsymbol{D} \cdot \boldsymbol{F}}{k_B T} C \right)$$
(2)

with particle flow velocity, u, particle diffusion coefficient tensor, D, external forces such as van der Waals interaction and body forces due to gravity, F, Boltzmann constant,  $k_B$ , and absolute temperature, T. Close to the surface ( $H \approx R$ ),  $C = C(\phi,R)$  becomes independent of H and signifies collision. Eq. (2) is numerically solved using finite difference method (see supplementary materials). The hydrodynamic drag on any adhered particle at any specific  $\phi$  is uniform due to axisymmetry, but changes as  $\phi$  varies. Particles are trapped when the surface attraction supersedes the hydrodynamic drag.

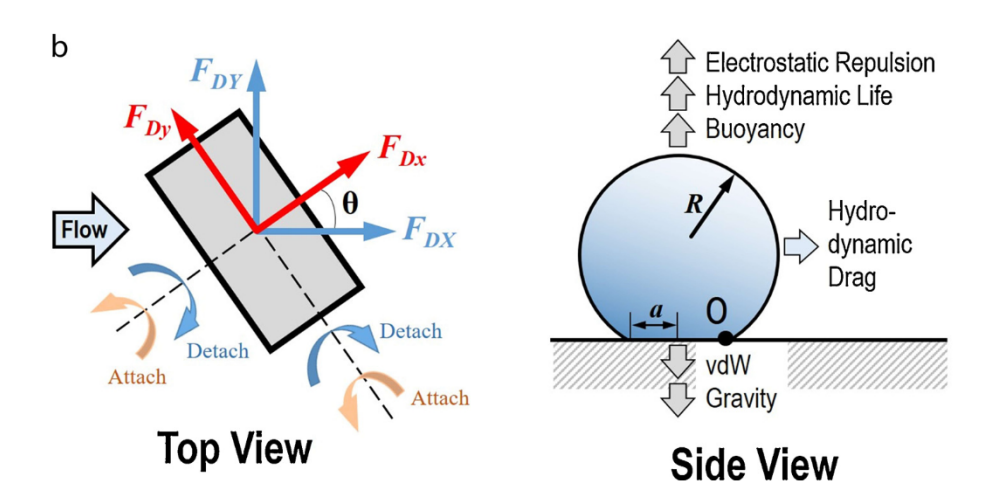
#### 2.2. Intersurface attraction

When a cylindrical particle with length, L, radius, R, elastic modulus, E, adheres to a rigid planar substrate, classical adhesion model [16] requires the net force per unit length to be

$$\frac{P}{L} = \underbrace{\frac{\pi E a^2}{4R}}_{Contact\ Force} + \underbrace{\frac{(\Delta \rho)g \cdot \pi R^2}{Bouyancy}}_{Bouyancy} + \underbrace{\frac{F_{CZ}}{Cohesive\ Zone}}_{without\ contact} + \underbrace{\frac{F_c}{Adhesion}}_{within\ contact}$$
(3)

The first term on RHS corresponds to the repulsive contact force that causes the cylinder to deform elastically [19]. The contact area is here a rectangle with width, 2a, and length, L. The net buoyant force,  $(\rho_s - \rho_l).g.V$  with  $\rho_s$  and  $\rho_l$  the densities of particle and water respectively, g the gravitational acceleration, and  $V = \pi R^2 L$  the particle volume, is negligibly small compared to other terms and is ignored hereafter. The hydrodynamic lift on a slender cylinder lying a planar substrate is also ignored. The intersurface force at the cell-collector interface gives rise to a cohesive zone immediate behind the contact edge ( $r \geq a$ ),  $F_{CZ} = F_{vdW} + F_{EDL}$ , with  $F_{vdW}$  the van der Waals attraction [20] and  $F_{EDL}$  the electrostatic double layer repulsion [21]. An adhesion force,  $F_c$ , is present within the contact area (r < a). At equilibrium, the net attraction ( $F_{CZ} + F_c$ ) is balanced by the repulsive contact force such that the

Fig. 2. (a) Sand grains in an ideal cubic packing configuration within the vertical filtration column. Streamline is shown over a single spherical collector. Hydrodynamic stress is uniform at specific  $\phi$  due to axisymmetry. (b) Top and side views of a single bacterial cell with a misorientation angle  $\theta$  to the flow. Hydrodynamic drag is derived by COMSOL. As external torque increases, the pivot of rolling moves to the contact edge (point O).



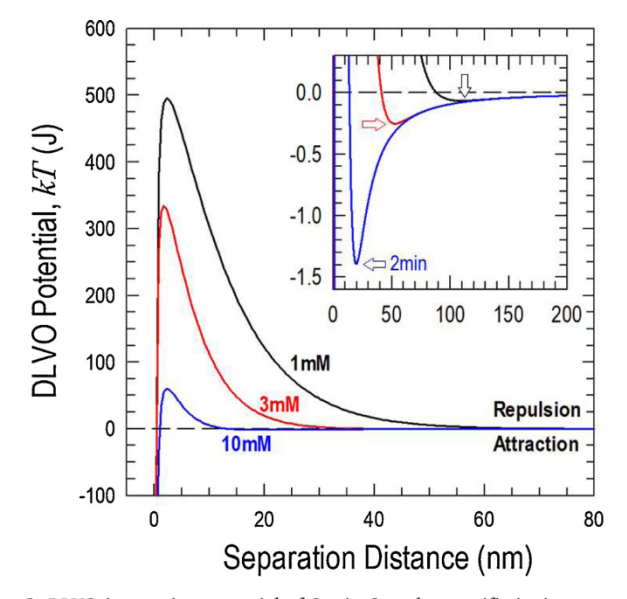


**Fig. 3.** DLVO interaction potential of Strain Q under specific ionic concentration. Repulsive barriers have heights in the range  $50-500\,k_B\,T$ , and  $2\min\,0.1-1.5\,k_B\,T$ . The inset shows details of the weak  $2\min$  (where arrows are pointing). The strong  $1\min$  is confined to 2nm from the substrate surface. Strain A has similar trend.

cell experience zero net force (P = 0).

To facilitate the computation efforts, the collector is treated as a flat substrate as the particle is two orders of magnitude smaller than the collector. The cylindrical particle has a projected rectangular area on the substrate 2RL, and is here taken to be  $\pi.a_b^2$  with  $a_b = (3L/4)^{1/3}a^{2/3}$  the equivalent radius. Based on the DLVO theory [17], the energy density per unit area is given by

$$V(z) = -\frac{A}{6\pi a_b z (1 + 14z/\lambda)} + \frac{\varepsilon_0 \varepsilon_r}{a_b} \left\{ 2\psi_p \cdot \psi_c \log\left(\frac{1 + e^{-\kappa z}}{1 - e^{-\kappa z}}\right) + (\psi_p^2 + \psi_c^2) \log(1 - e^{-2\kappa z}) \right\}$$
(4)

with A the Hamaker constant, z=z(r) the intersurface separation between particle and collector at a radial distance r from the contact edge,  $\lambda$  a characteristic wavelength of the dielectric,  $\varepsilon_0$  the permittivity of free space,  $\varepsilon_r$  the dielectric constant of electrolyte,  $\psi$  the surface potential, and the subscripts p and c denoting the particle and collector respectively. The disjoining pressure given by P(z)=dV(z)/dz comprises a strong but short-ranged primary minimum (1min) and a weak but long-ranged secondary minimum (2min), separated by a repulsive barrier denoted by subscript R, as shown in Figs. 3 and 4. Further simplification is made by the Dugdale-Barenblatt-Maugis (DBM)

approximation [22,23] where the disjoining pressure is a function with constant force magnitudes and ranges in each zone,

$$p(z) = \begin{cases} -p_1 & \text{for } z_0 < z \le z_1, \ a < r \le c_1 \ 1min \\ p_R & \text{for } z_1 < z \le z_R, \ c_1 < r \le c_R \ Energy \ barrier \\ -p_2 & \text{for } z_R < z \le z_2, \ c_R < r \le c_2 2min \\ 0 & \text{for } z > z_2, \ r > c_2 \end{cases}$$
 outside CZ (5)

where r is radial distance from the symmetric axis,  $z_0$  the equilibrium spacing,  $z_1, z_R$  and  $z_2$  are force ranges, and  $\xi_1, \xi_R$  and  $\xi_2$  are normalized radii of 1 min, barrier, and 2 min respectively (Fig. 4). For Strain Q in the presence of 3 mM KCl (aq),  $p_1$  is in  $\sim 10^3$  Pa being effective in a range of  $z\sim 2$  nm, the repulsive barrier in  $10^{-2}\sim 10$  Pa, and 2 min in  $10^{-2}\sim 10$  Pa being effective in of  $10\sim 100$  nm. For simplicity, all radial distances are normalized with respect to a such that  $\zeta=r/a$  for r< a within the contact edge and  $\xi=r/a$  for  $r\geq a$  without the contact edge. The net force on the particle is therefore a competition of the three zones subject to ion strength variation, and can be written as

$$\frac{F_{CZ}}{a} = \underbrace{p_1(\xi_1 - 1)}_{1min} - \underbrace{p_R(\xi_R - \xi_1)}_{Energy \ Barrier} + \underbrace{p_2(\xi_2 - \xi_R)}_{2min} \tag{6}$$

The adhesion force within the contact ( $\zeta$  < 1) is given by

$$Fc = \int_0^1 (\sigma 1 + \sigma R + \sigma 2) d\varsigma \tag{7}$$

with the induced stresses given by

$$\sigma_{1}(\zeta) = -\int_{1}^{\xi_{1}} p_{1} \times g(\zeta, \xi) d\xi$$

$$\sigma_{R}(\zeta) = \int_{\xi_{1}}^{\xi_{R}} p_{R} \times g(\zeta, \xi) d\xi$$

$$\sigma_{2}(\zeta) = -\int_{\xi_{R}}^{\xi_{2}} p_{2} \times g(\zeta, \xi) d\xi$$
(8)

with the Green's function [16,24,25]

$$g(\zeta,\xi) = \frac{a}{\pi} \times \sqrt{\frac{1-\zeta^2}{\xi^2 - 1}} \times \left(\frac{1}{\xi - \zeta} + \frac{1}{\xi + \zeta}\right)$$
(9)

The gap between the deformed cylinder and rigid substrate follows the Hertz contact theory,

$$z(\xi) = \frac{a^2}{2R} \times (\xi, \sqrt{\xi^2 - 1} - \cosh^{-1}\xi)$$
 (10)

with the boundary conditions:  $z(\xi_1) = z_1$ ,  $z(\xi_R) = z_R$ , and  $z(\xi_2) = z_2$ . The net adhesion force becomes

$$\begin{split} \frac{F_a}{a} &= 2p_1 \times \sqrt{\xi_1^2 - 1} - 2p_R \times (\sqrt{\xi_R^2 - 1} - \sqrt{\xi_1^2 - 1}) \\ &- 2p_2 \times (\sqrt{\xi_2^2 - 1} - \sqrt{\xi_R^2 - 1}) \end{split} \tag{11}$$

It is remarked that the present model requires the adhered particle to experience the attractive surface forces at both 1 min and 2 min as

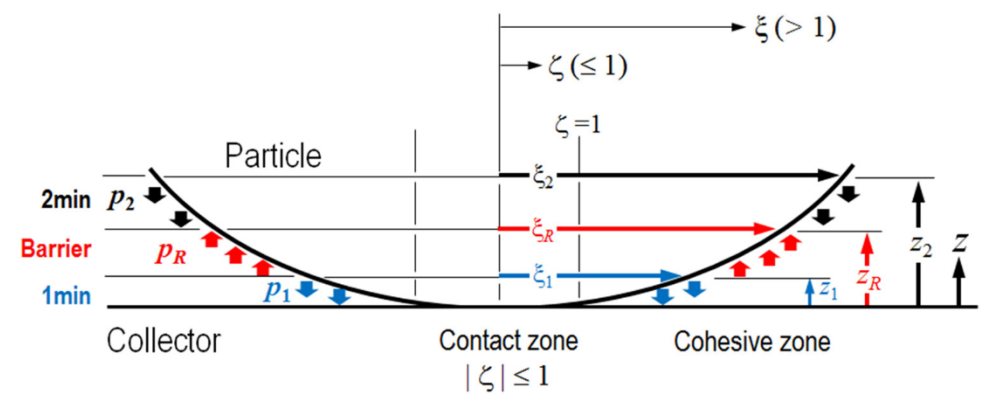


Fig. 4. Surface forces on the bacterial surface due to DLVO potential, showing the attractive 1min and 2min and repulsive barrier.

well as the repulsive energy barrier, which is not accounted for by existing model in the literature [15].

#### 2.3. Hydrodynamic drag

Some cells collide with the collector surface and are stuck as a result of intersurface attraction, while others escape and are carried away along the streamlines. Rather than an ensemble of sand collector stacked in specific configuration, we consider a single collector subject to an external uniform flow is modeled. As the adhering particles are small compared to the collector diameter, they lie flat on the planar substrate and are subjected to the external flow. Based on Happel's sphere-in-cell model [14,26],  $F_D(\phi)$  vanishes at the stagnation points at  $\phi = 0^\circ$  and  $\phi = 180^\circ$ , but reaches its maximum  $(F_D)_{max}$  at  $\phi = 90^\circ$ . Force at an arbitrary angle  $\phi$  is given by

$$F_D(\varphi) = (F_D)_{max} \times \sin \varphi \tag{13}$$

Simulation is performed using COMSOL. Liquid flows through a channel with a large rectangular cross section to ensure uniform velocity. Several boundary conditions are reinforced: (i) streamline is parallel to the channel axis or X-axis, (ii) pressure at the outlet is negligible, (iii) no slippage at the channel wall. Meanwhile, individual cell adheres on the collector surface in a stochastic manner, its axis subtends a random misorientation angle,  $\theta$ , to the streamline as shown in the Fig. 2b. The minor-major axes are along the x-y direction respectively. The effective hydrodynamic drag therefore depends on both angles  $F_D = F_D(\phi,\theta)$ . At a fixed  $\phi$ , cylindrical cell aligns with the streamline  $(\theta = 0^{\circ})$  experience negligible drag, while those perpendicular to the flow  $(\theta = 90^{\circ})$  is subject to maximum drag. The hydrodynamic stress on the particle in X, Y, Z directions are calculated using a customized tetrahedral mesh, and the net forces,  $F_{DX}(\theta)$  and  $F_{DY}(\theta)$ , are derived by integrating stress over the particle surface.

To model detachment, the average velocity, u, is taken to be uniform across the channel cross section, and the streamlines are parallel to the channel axis or the X-axis. The X-Y plane subtends an angle  $\theta$  from the X-Y plane, and the hydrodynamic drag becomes

$$\begin{bmatrix} F_{Dx} \\ F_{Dy} \end{bmatrix} = \begin{bmatrix} \cos \theta & -\sin \theta \\ \sin \theta & \cos \theta \end{bmatrix} \begin{bmatrix} F_{DX} \\ F_{DY} \end{bmatrix}$$
(14)

Once a particle detaches, it can roll, slide or lift [13,15]. The dominant mode rolling takes place in either longitudinal or transverse direction depending on the orientation of the particle axis. At  $\theta=0^\circ$ , the streamlined particles align with the flow and is subjected to the least shear even at a high flowrate. A small misorientation leads to small torque on the particle which is now susceptible to roll about the major axis. In case of  $\theta=90^\circ$ , shear on the particle is the maximum. Increasing u raises  $F_D$ , and the rolling pivot moves towards the edge of the contact area. A simple detachment criterion can be established based on the induced torque,  $\Gamma$ , defined to be the product of the net adhesion force and moment arm roughly the effective particle radius. Detachment occurs once  $\Gamma$  exceeds the thresholds,

$$\Gamma_{||} = F_{D||} \times R \ge F_a \times a \text{ for } \theta \approx 0^{\circ}$$
 (15a)

$$\Gamma_{\perp} = F_{D\perp} \times R \ge F_a \times L / 2 \text{ for } \theta \approx 90^{\circ}$$
 (15b)

Apparently  $\Gamma_{||} >> \Gamma_{\perp}$ , and the particle likely to roll about the major axis rather than the minor axis. Torque due to  $\Gamma_{||}$  is therefore irrelevant in the present context. Whether a particle detaches depends on  $\theta$  and the subsequent  $\Gamma_{\perp}$ . For a specific adhesion strength, particles with misorientation angle  $-\theta^* < \theta < \theta^*$  remain trapped on the collector surface, where  $\theta^*$  is the threshold such that external torque is balanced by adhesion. Particles with  $|\theta| > \theta^*$  will be washed away by the flow. At a specific meridional angle  $\phi$  with respect to the collector surface (c.f. Fig. 2b), the local flow velocity is given by  $u.\sin \phi$ , and  $G(\theta_i u.\sin \phi)$  is the particle distribution function of  $\theta$ , and is assumed to

be Gaussian. The mean and standard deviation are measured by the microfluidic device (see Section 2.4.3). Thus,  $\theta^*$  is a function of  $\phi$ , and the filtration efficiency is given by

$$\alpha = \frac{\int_0^{\pi} \int_0^{\theta * (\phi)} G(\theta, u. \sin \phi) \times C(\phi, H) \times 2\pi R. \sin \phi. R. d\theta. d\phi}{\int_0^{\pi} C(\phi, H) \times 2\pi R. \sin \phi. R. d\phi}$$
(16)

which is valid for either 1 min or 2 min. To account for both 1 min and 2 min, the overall attachment efficiency can be written as

$$\alpha = \alpha_{1\min} \times f_{1\min} + \alpha_{2\min} \times f_{2\min}$$
 (17)

where f is the initial fraction of particles falling into the energy wells.

## 2.4. Experimental determination of filtration efficiency

#### 2.4.1. Bacteria strains

Two bacterial strains related to environment and human health are investigated and fitted to the mathematical model. They are chosen because they have similar dimension, geometry, and mechanical behavior (e.g. elastic modulus), but vastly different adhesion behavior as shown in our previous study [27], and will serve as good control experiment for comparison purposes.

- (a) Gram-negative *Aeromonas punctata* (abbr. Strain Q) is associated with human diseases including gastroenteritis, cellulitis and diarrhea. The physical dimensions are given by length (major axis)  $1.28\pm0.70~\mu\text{m}$ , width (minor axis)  $0.78\pm0.15~\mu\text{m}$ , aspect ratio  $1.65\pm0.80$ , and elastic modulus  $244\pm41~\text{kPa}$ ;
- (b) Gram-negative *Raoultella ornithinolytica* (abbr. Strain A) is a major cause of histamine fish poisoning [28], with length, width and aspect ratio given respectively by  $1.58\pm0.39~\mu m$ ,  $0.80\pm0.09~\mu m$ , and  $1.98\pm0.5$ , and elastic modulus  $237\pm42~kPa$ . Both strains are grown aerobically at 37~C in 25~g/L Luria-Bertani (LB) medium (Sigam-Aldrich, Inc., St. Louis, MO). To eliminate the potential impact of the growth stage on bacterial micro adhesion properties [27], all sample cells are in stationary 16-18~h growth phase.

## 2.4.2. Column tests

Fig. 1 shows the column test [27]. Ultrapure silica sand grains, GRANUSIL 4095 (UNIMIN Corp., LeSueur, MN), with a nominal diameter of 289 µm serve as collector. The grains are cleansed using 1 mM NaOH (aq) for 24 h, rinsed with deionized (DI) water, dried in an oven at 103 °C for 24 h, then left in an oven at 550 °C for 1 h before being packed in a sterile cylindrical glass syringe (column) with an inner diameter of 2.67 cm to a height of 10 cm. Porosity of the sand column, defined as the volume ratio of void to bulk solid, is determined by conventional gravimetric method to be 0.40, sufficiently close to the ideal value of 0.467 in close cubic packing. DI water of 20 pore volumes (PV, with 1 PV = 24 mL) flushes through the column, followed by 10 pore volume of background electrolyte of 3 mM KCl (aq) at flowrate in the range of  $Q = 5 \,\text{mL/min}$ , which is equivalent to a flow speed of V = 0.015 cm/s, until a steady state is established. Bacteria suspended in the same background electrolyte is then pumped for 3-4 PV, followed by  $\sim 3 \,\mathrm{PV}$  of bacteria-free pure electrolyte at the same V. A magnetic stirrer ensures uniform distribution of bacteria in the influx. The initial bacteria concentration,  $C_0$ , is measured by a UV-vis spectrophotometer with wavelength  $\lambda = 500 \, \text{nm}$  (Model UV Mini 1240 Shimadzu, Kyoto, Japan) right before the experiment begins. The spectrophotometer essentially measures only the absorbance of the sample, but the quantity is directly proportional to the number density per unit volume. In this study, only the density ratio, rather than the exact number density, is needed. At the efflux, concentration is monitored throughout the experiment using a UV-vis spectrophotometer (model UV Mini 1240 Shimadzu, Kyoto, Japan). Experiments were repeated for combinatorial of (i)  $Q = 5 \sim 50$  mL/min or V = 0.015 cm/s  $\sim 0.15$  cm/s with stepwise increment of 5 mL/min and (ii) ionic concentration of 1, 3 and 10 mM.

#### 2.4.3. Microfluidic measurement

The column test represents a macroscopic measurement of  $\boldsymbol{\alpha}$  despite being time consuming and costly. We earlier designed a microfluidic device allowing a rapid measurement of  $\alpha$  [29]. In essence, a simple single channel is fabricated in PDMS and is flushed with background KCl (aq) with desirable ionic concentration from one end to the other. At the channel midspan, a bacterial rich solution is introduced into the channel at zero flow and the cells are allowed to settle. The setup sits on an inverted optical micrograph to monitor the distribution and orientation of the ellipsoidal bacterial cells. Flow of background solution at desirable flowrate then resumes to wash off the loosely bounded cells leaving behind the firmly trapped. Misorientation angle of the cell ensemble left on the glass substrate was measured by standard image analysis code. Number of particles within a small range of misorientation was then fit to a Gaussian distribution curve. It should be emphasized that the microfluid measurement has a different configuration compared with the column test. Here the glass substrate is continuous and planar, and the surface boundary layer is well defined. The column, on the other hand, comprises stacked collectors and the bacteria has to pass through the complex percolated channels. Results from the two tests can be compared qualitatively and empirically correlated.

#### 3. Results

With all the relevant parameters entered into the governing equations and computation codes as described above,  $\alpha$  was derived as a function of flowrate and ionic concentration. Table 1 shows the critical torque required to detach a particle lying in longitudinal or transverse direction to the flow, as well as the hydrodynamic torque, for a range of ionic concentrations and particle axis being parallel or orthogonal to the flow direction. Only critical hydrodynamic torque  $\Gamma^*(\varphi = 90^\circ)$  is listed for typical groundwater flowrate of Q = 5 - 25 ml/min, and  $\Gamma^*$  at other  $\varphi$  is found by Eq. (13). Critical torque to remove particles trapped in 2 min is roughly two orders of magnitude smaller than the hydrodynamic drag. These particles are only loosely attached to the collector and are washed away in the presence of a relatively slow flow. For those particles trapped in 1 min,  $\Gamma^*$  is comparable to the external torque. It is noted that  $\Gamma_{||} < \Gamma_{\perp}$ , detachment from 1 min will more likely happen in the longitudinal direction. Filtration efficiency essentially depends on how many particles trapped in 1 min are retained and how many are washed off.

The critical misorientation angle is computed as a function of meridional angle and flow rate,  $\theta^*(\varphi,Q)$ , as shown in Fig. 5a–b for the two bacterial strains. In case of infinite attractive intersurface force or zero flowrate, all particles will be retained on the collector surface and  $\theta^* = 90^\circ$ , and the filtration efficiency is 100 %. In reality, adhesion strength is limited. In Fig. 5a, Strain Q in 3 mM KCl (aq) at 50 mL/min has  $\theta^* = 90^\circ$  for  $0 < \varphi < \varphi^*$  with the threshold  $\varphi^* = 23^\circ$ , in that, the hydrodynamic stress is too small to detach any cells in the vicinity of the stagnant point ( $\varphi = 0^\circ$ ) bounded by  $\varphi < \varphi^*$  even when the particle axis is perpendicular to flow. For  $\varphi = \varphi^*$ , particles with axis

perpendicular to the streamline ( $\theta^* = 90^\circ$ ) will be detached but those with small misorientation will be retained. For  $\phi > \phi^*$ , increasing torque pulls the particles with  $\theta \ge \theta^*$  off the substrate, with  $\theta^*$  shown in Fig. 5a. As the surface forces cannot trap all the particles on the collectors and the filtration efficiency deteriorates. At a smaller flowrate, both  $\varphi^*$  and  $\theta^*$  are pushed to higher values as more particles subjected to smaller shear remain on the collector. It is quite remarkable that should Q reduce from 50 to 10 mL/min, φ\* increases drastically from  $\sim 25^{\circ}$  to  $\sim 80^{\circ}$ . There exists a lower bound of flowrate where no particle will detach. A lower ionic concentration (1 mM) raises the repulsive barrier in the DLVO potential but reduces the 2 min well. The resulting  $\theta^*(\phi,Q)$  spreads over a large range of  $\phi$ :  $\phi^*(1 \text{ mM}) > \phi^*(3 \text{ mM})$ mM) at Q = 20 mL/min, but  $\phi^*(1 \text{ mM}) < \phi^*(3 \text{ mM})$  at Q = 50 mL/min. In a more concentrated solution (10 mM), the energy barrier is significantly lowered and 2 min deepens, and \$\phi^\*(10 mM)\$ rises above φ\*(3 mM) at all flowrate. Results for Strain A is shown in Fig. 5b. Strain Q is apparently more adhesive than A and is expected to lead to higher filtration efficiency.

To determine  $\alpha$ , Eq. (16) is solved based on three key parameters, namely,  $\theta^*(\phi,Q)$ ,  $G(\theta,u)$  and  $C(\phi)$ . The function  $G(\theta,u)$  is determined experimentally using the microfluidic device. After the particles are settled on the substrate in stagnant fluid, flow removes a proportion of those with  $\theta > \theta^*$  leaving behind those with small  $\theta$ . A Gaussian distribution with mean at  $\theta = 0^\circ$  and standard deviation  $\sigma$  is assumed for  $\theta$ .

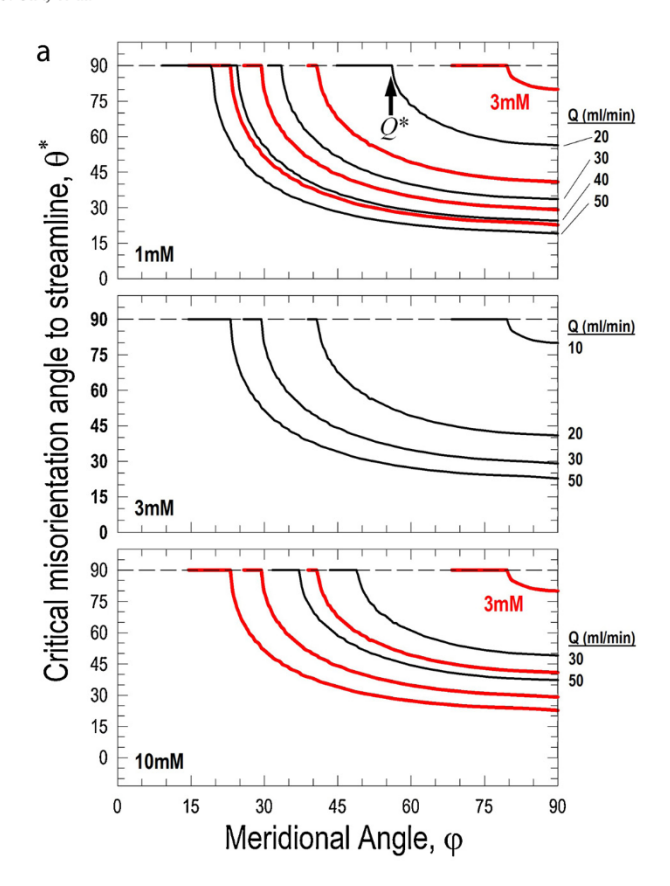
$$G = \frac{1}{\sqrt{2\pi\sigma^2}} \exp\left(-\frac{\theta^2}{2\sigma^2}\right), -\frac{\pi}{2} \le \theta \le \frac{\pi}{2}$$
(18)

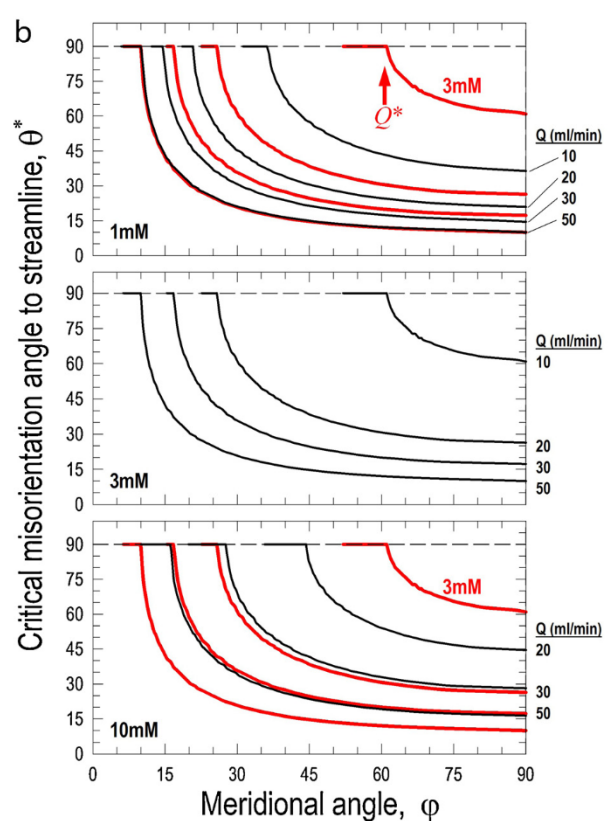
Fig. 6 shows experimental data for Strain Q at 3 mM KCl (aq) under two flowrates, with  $\sigma(Q=5\,\mathrm{mL/min})=75^\circ$  and  $\sigma(Q=5\,\mathrm{mL/min})=40^\circ$ . Higher flowrate obviously removes more particles and leaves behind the ones more aligned with the streamline, leading to a narrower Gaussian distribution. The measurements are confined to 1, 3, and 10 mM KCl (aq) due to the high cost in this study. Assuming a linear relation between  $\sigma$  and Q, the intermediate values are found by interpolation. We resort to experimental measurement to determine the function  $C(\varphi,H)$ . Firstly, it is chosen  $H\approx 100\,\mathrm{nm}$ , which is the range of DLVO surface force range. By numerically solving the convection-diffusion equation using finite difference method [18],  $f_{1\min}$  and  $f_{2\min}$  can be estimated by fitting the model to the column test measurements. As ionic concentration increases, higher fraction of particles overcomes the energy barrier to reach 1 min, as shown in Table 2.

Fig. 7 shows the experimental filtration efficiency obtained from column test as a function of flowrate in various ionic concentrations, which shows consistency with the model. A sudden drop of  $\alpha$  was expected at a critical value of  $Q^*$  for all ionic concentration as the hydrodynamic stress is just sufficient to detach the adhered particles. Strain A showed higher  $\alpha$  and  $Q^*$  than Strain Q at the same ionic concentration. It is expected that the phenotype of bacterial strains will influence the filtration behavior. Contrasting the classical CFT, the current model provides better comprehension of the underlying physics

**Table 1** Critical torques  $\Gamma_{||}$  and  $\Gamma_{\perp}$  (N·m) to detach an adhered particle with its axis parallel and perpendicular to the streamline. The hydrodynamic torque is also shown in the two directions, with the lower and upper bounds corresponding to Q = 5 mL/min and 50 mL/min respectively.

Bacterial strain	Ionic strength KCl (aq)	Critical torque to overcome 1 min $(10^{-20} \text{ N.m})$		Critical torque to overcome $2  \text{min}$ ( $10^{-20}  \text{N.m}$ )		Torque due to hydrodynamic shear $(10^{-20} \text{ N.m})$	
		$\Gamma_{  }$	$\Gamma_{\!\perp}$	$\Gamma_{  }$	$\Gamma_{\!\perp}$	$\Gamma_{  }$	$\Gamma_{\perp}$
Aeromonas punctata	1 mM	58.1	3850	0.0737	0.0198	0.007 ~ 190	0.05 ~ 130
(Q)	3 mM	68.8	3560	0.425	0.170		
	10 mM	106	4130	2.33	1.06		
Raoultella ornithinolytica (A)	1 mM	36.1	3430	0.869	0.0178	$0.1 \sim 200$	$0.01 \sim 100$
	3 mM	36.7	3490	0.546	0.178		
	10 mM	57.6	4500	2.63	0.970		





**Fig. 5.** Theoretical critical misorientation angle,  $\theta^*$ , at detachment over a range of ionic concentration and flow rate for (a) Strain Q and (b) Strain A. Results of 3mM are plotted in other graphs as comparison.

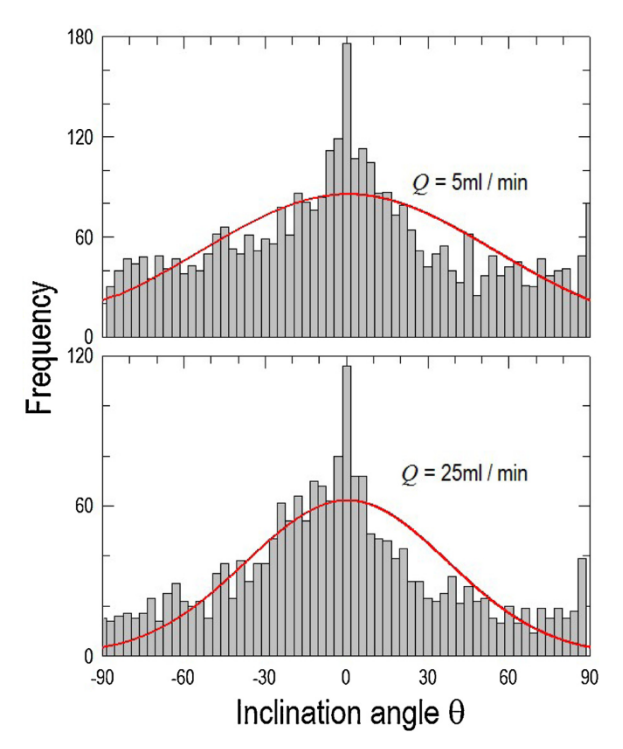


Fig. 6. Experimental distribution of misorientation angle in the presence of low and high flowrate for Strains Q in 3 mM KCl (aq) at steady state. Data are fitted to Gaussian function. Spread in  $\theta$  is drastically reduced at high flow rate.

**Table 2** Fraction,  $f_{1\min}$ , of strain A and strain Q left on the glass substrate in the microfluidic device after being subject to maximum shear in KCl (aq) of indicated concentration. Increase in  $f_{1\min}$  was seen in more concentrated solution.

Bacterial strain	1 mM	3 mM	10 mM
Aeromonas punctata (Q)	29.78 %	40.62 %	52.65 %
Raoultella ornithinolytica (A)	29.27 %	40.88 %	43.00 %

and mechanics that is experimentally verifiable.

## 4. Discussion and significance

Tufenkji et al. [30] investigated colloidal filtration of polystyrene particles in a sand packed column, and showed deposition of roughly 5% of the particles in 1 min in 3 mM KCl (aq), which is much lower than our measurement (c.f. Table 2). One explanation is the surface charge heterogeneity on particle and collector, which is in fact inevitable in our bacterial strains. A fraction of bacteria is therefore expected to experience smaller energy barrier. Moreover, bacterial motility [10,11], cell surface substances (CSS) [27,28], and folding of the bacterial appendages under high ionic concentration [31], can effectively influence the particle-substrate separation and thus the intersurface forces and ultimate filtration. It is recognized that our model is incapable of capturing the comprehensive properties of living bacteria in full details. There are other limitations and shortcomings. A comprehensive model in the future should comprise the stacking configuration of the collectors, their stochastic dimension, their deviation from spherical geometry and surface roughness. These factors have significant impacts on the particles as they flow through the percolated channels in the porous medium and to circumvent the obstacles. Even in case of steady flow, the complex flow involves the many stagnant points and slow flow in the wake or leeside of the collectors, let alone the complex geometry of the boundary layer on the surface of the now stacked collectors. Another element not discussed is the detail diffusion of particles entering

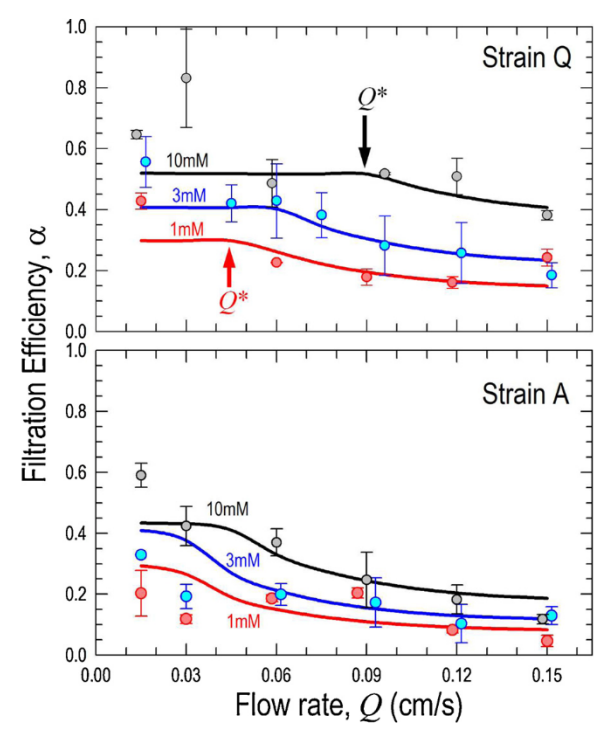


**Fig. 7.** Attachment efficiency derived by the new model for strain A and Q. Solid line and dash lines indicate the results of the new model. The symbols indicated column test results under varying flow rates and ionic concentrations.

and leaving the force field of interaction potential, which at least accounts for how the particles first come into contact with the collector surface in case of a high energy barrier. Size of the collector grains also plays a role especially when the particles aggregate into a large entity. In case of small collectors, the closely packed column narrows the percolated channels and thus hinders the passage of large aggregates.

The present model is applicable to rigid non-deformable colloidal particles even without intimate contact with the substrate. The celebrated Johnson-Kendall-Roberts (JKR) adhesion model used in the colloid literature [15] requires either zero range contact force with  $c_2$ = a in Eq. (5) or an "equivalent" non-zero contact radius. Here we adopt the cohesive zone model for long-range forces even for zero contact or a = 0. In fact, Eq. (5) presents a long range for the DLVO electrostatic double layer such that  $F_{CZ}$  in Eq. (3) is a summation of intersurface forces from the contact edge (r = a) to an ideal infinite distance  $(r > c_2)$  where there is no direct contact between the surfaces. In case of a = 0, there is no elastic energy stored in the particle and  $F_c$ = 0 in Eq. (3), and the torque required to detach the particle is therefore the net force  $F_{CZ}$  multiplied by the apparent moment arm ( $c_2$  – a) where a can be zero. The cohesive zone description and Green's function method can be applied to any general short-range or longrange intersurface interactions, which is beyond the scope of this paper.

The net adhesion force on the bacterial cells in this study is roughly 3 orders of magnitude higher than that spherical colloidal particles in Shen's work [14]. This further shows that rod shape cells / particles and the aspect ratio can have significant consequences in filtration. Contrasting CFT, the present model delves into the underlying fundamental mechanism comprising intersurface forces and their dependence on ionic concentration, elastic deformation of particles due to adhesion, hydrodynamic shear and torque due to flow velocity, and geometry of both particle and collector. Particles detach from the collector surface depends on whether the hydrodynamic shear overcome the interfacial adhesion at a specific meridional-azimuthal location of the spherical collector. The percentage of particles stayed adhered thus determines the filtration efficiency. Measurements in the two specific bacterial strains using the microfluidic device and the conventional column test

shows consistency with the computational results. It is remarkable that the classical DLVO electrostatic double layer description is sufficient to account for the behavior of Q and A. It is therefore possible to extend the Green's function method to other force laws such as the steric attraction-repulsion at the molecular scale at the particle-substrate interface. Despite a number of aforementioned essential factors being left out in the model, the present work shows the indispensable role of solid-mechanics and adhesion-detachment mechanics thus derived in filtration. It also provides a mechanistic understanding of transport behavior of microorganisms upon flowrate and ion concentration in typical groundwater and surface flows. Such information is crucial in designing effective water filtration systems and bioremediation. The interfacial adhesion model also provides a basis to discuss biofilm formation

## CRediT authorship contribution statement

Jianfeng Sun: Conceptualization, Data curation, Formal analysis, Investigation, Methodology, Software, Validation, Visualization, Writing - review & editing. Ran Ran: Data curation, Investigation, Validation. Sinan Muftu: Conceptualization, Funding acquisition, Methodology, Resources, Writing - review & editing. April Z. Gu: Funding acquisition, Methodology, Resources, Supervision, Writing - review & editing. Kai-Tak Wan: Conceptualization, Funding acquisition, Methodology, Project administration, Resources, Supervision, Validation, Writing - original draft, Writing - review & editing.

#### **Declaration of Competing Interest**

The authors declare that they have no known competing financial interests or personal relationships that could have appeared to influence the work reported in this paper.

## Acknowledgements

The authors are grateful to the financial support by National Science Foundation CMMI#1333889. Any opinions, findings, and conclusions or recommendations expressed in this material are those of the authors and do not necessarily reflect the views of NSF.

## Appendix A. Supplementary data

Supplementary material related to this article can be found, in the online version, at doi:https://doi.org/10.1016/j.colsurfa.2020.125169.

## References

- N. Tufenkji, J.N. Ryan, M. Elimelech, Peer reviewed: the promise of bank filtration, Environ. Sci. Technol. 36 (21) (2002) 422A–428A.
- [2] A. Dehkharghani, N. Waisbord, J. Dunkel, J.S. Guasto, Bacterial scattering in microfluidic crystal flows reveals giant active Taylor–Aris dispersion, Proc. Natl. Acad. Sci. U. S. A. 116 (23) (2019) 11119.
- [3] K.-M. Yao, M.T. Habibian, C.R. O'Melia, Water and waste water filtration. Concepts and applications, Environ. Sci. Technol. 5 (11) (1971) 1105–1112.
- [4] T. Iwasaki, J.J. Slade, W.E. Stanley, SOME NOTES ON SAND FILTRATION [with Discussion], Journal (American Water Works Association) 29 (10) (1937) 1591–1602
- [5] R. Rajagopalan, C. Tien, Trajectory analysis of deep-bed filtration with the sphere-in-cell porous media model, AIChE J. 22 (3) (1976) 523–533.
- [6] N. Tufenkji, M. Elimelech, Correlation equation for predicting single-collector efficiency in physicochemical filtration in saturated porous media, Environ. Sci. Technol. 38 (2) (2004) 529–536.
- [7] R.J. Steffan, K.L. Sperry, M.T. Walsh, S. Vainberg, C.W. Condee, Field-scale evaluation of in situ bioaugmentation for remediation of chlorinated solvents in groundwater", Environ. Sci. Technol. 33 (16) (1999) 2771–2781.
- [8] C. Ferguson, A.Md.R. Husman, N. Altavilla, D. Deere, N. Ashbolt, Fate and transport of surface water pathogens in watersheds, Crit. Rev. Environ. Sci. Technol. 33 (3) (2003) 299–361.
- [9] M.W. Becker, S.A. Collins, D.W. Metge, R.W. Harvey, A.M. Shapiro, Effect of cell physicochemical characteristics and motility on bacterial transport in groundwater, J. Contam. Hydrol. 69 (3-4) (2004) 195–213.

- [10] T.A. Camesano, B.E. Logan, Influence of fluid velocity and cell concentration on the transport of motile and nonmotile bacteria in porous media, Environ. Sci. Technol. 32 (11) (1998) 1699–1708.
- [11] M. Hendry, J. Lawrence, P. Maloszewski, Effects of velocity on the transport of two bacteria through saturated sand, Ground Water 37 (1) (1999) 103–112.
- [12] V.I. Syngouna, C.V. Chrysikopoulos, Transport of biocolloids in water saturated columns packed with sand: effect of grain size and pore water velocity, J. Contam. Hydrol. 126 (3-4) (2011) 301–314.
- [13] J. Bergendahl, D. Grasso, Prediction of colloid detachment in a model porous media: hydrodynamics, Chem. Eng. Sci. 55 (9) (2000) 1523–1532.
- [14] C. Shen, Y. Huang, B. Li, Y. Jin, Predicting attachment efficiency of colloid deposition under unfavorable attachment conditions, Water Resour. Res. 46 (11) (2010).
- [15] S. Torkzaban, S.A. Bradford, S.L. Walker, Resolving the coupled effects of hydrodynamics and DLVO forces on colloid attachment in porous media, Langmuir 23 (19) (2007) 9652–9660.
- [16] K. Johnson, J. Greenwood, Maugis analysis of adhesive line contact, J. Phys. D Appl. Phys. 41 (19) (2008) 199802.
- [17] J.A. Redman, S.L. Walker, M. Elimelech, Bacterial adhesion and transport in porous media: role of the secondary energy minimum, Environ. Sci. Technol. 38 (6) (2004) 1777–1785.
- [18] M. Elimelech, Particle deposition on ideal collectors from dilute flowing suspensions: Mathematical formulation, numerical solution, and simulations, Sep. Technol. 4 (4) (1994) 186–212.
- [19] M.K. Chaudhury, T. Weaver, C.Y. Hui, E.J. Kramer, Adhesive contact of cylindrical lens and a flat sheet, J. Appl. Phys. 80 (1) (1996) 30–37.
- [20] J. Gregory, Approximate expressions for retarded van der Waals interaction, J. Colloid Interface Sci. 83 (1) (1981) 138–145.
- [21] R. Hogg, T.W. Healy, D. Fuerstenau, Mutual coagulation of colloidal dispersions,

- Trans. Faraday Soc. 62 (1966) 1638-1651.
- [22] K.-T. Wan, B.R. Lawn, Effect of chemical interaction on barenblatt crack profiles in brittle solids, Acta Metall. Mater. 40 (12) (1992) 3331–3337.
- [23] J. Sun, S. Muftu, A.Z. Gu, K.-T. Wan, Intersurface adhesion in the presence of capillary condensation, J. Appl. Mech. 85 (6) (2018) 061009, https://doi.org/10.1115/1.4039621.
- [24] H. Westergaard, Bearing pressures and cracks, J. Appl. Mech. 18 (1939).
- [25] H. Tada, P. Paris, G. Irwin, Handbook for stress analysis of cracks, Del Res. (1985).
- [26] J. Happel, Viscous flow in multiparticle systems: slow motion of fluids relative to beds of spherical particles, AICHE J. 4 (2) (1958) 197–201.
- [27] Y. Li, X. Wang, A. Onnis-Hayden, K.T. Wan, A.Z. Gu, Universal quantifier derived from AFM analysis links cellular mechanical properties and cell-surface integration forces with microbial deposition and transport behavior, Environ. Sci. Technol. 48 (3) (2014) 1769–1778.
- [28] X. Wang, Y. Li, A. Onnis-Hayden, C. Gao, A.Z. Gu, K.T." Wan, Correlation of macroscopic aggregation behavior and microscopic adhesion properties of bacteria strains using a dimensionless Tabor's parameter, J. Colloid Interface Sci. 374 (1) (2012) 70-76
- [29] J. Sun, N. Tandogan, A. Gu, S. Müftü, E. Goluch, K.-T. Wan, Quantification of colloidal filtration of polystyrene micro-particles on glass substrate using a microfluidic device, Colloids Surf. B Biointerfaces 165 (5) (2018) 381–387, https://doi. org/10.1016/j.colsurfb.2018.02.044.
- [30] N. Tufenkji, M. Elimelech, Deviation from the classical colloid filtration theory in the presence of repulsive DLVO interactions, Langmuir 20 (25) (2004) 10818–10828.
- [31] I.E. Ivanov, Influence of Ionic Strength on Elasticity of Bacterial Cell Surface Appendages As Characterized by Quantitative Nanomechanical Atomic Force Microscopy, (2012).